

RESEARCH ARTICLE

10.1002/2014JA020180

Key Points:

- High correlation between dayside diffuse aurora and solar wind dynamic pressure
- Indication of generation of the dayside diffuse aurora by the dayside chorus
- Dayside diffuse auroral intensity is modulated by the compressional pulsations

Correspondence to:

Z.-J. Hu and B. Ni,
huzejun@pric.org.cn;
bbni@whu.edu.cn

Citation:

Shi, R., Z.-J. Hu, B. Ni, D. Han, X.-C. Chen, C. Zhou, and X. Gu (2014), Modulation of the dayside diffuse auroral intensity by the solar wind dynamic pressure, *J. Geophys. Res. Space Physics*, 119, 10,092–10,099, doi:10.1002/2014JA020180.

Received 13 MAY 2014

Accepted 21 NOV 2014

Accepted article online 26 NOV 2014

Published online 31 DEC 2014

Modulation of the dayside diffuse auroral intensity by the solar wind dynamic pressure

Run Shi^{1,2}, Ze-Jun Hu¹, Binbin Ni³, Desheng Han¹, Xiang-Cai Chen^{4,5,6}, Chen Zhou³, and Xudong Gu³

¹SOA Key Laboratory for Polar Science, Polar Research Institute of China, Shanghai, China, ²Department of Mathematics and Statistics, Memorial University of Newfoundland, St. John's, Newfoundland, Canada, ³Department of Space Physics, School of Electronic Information, Wuhan University, Wuhan, Hubei, China, ⁴University Centre in Svalbard, Longyearbyen, Norway, ⁵Department of Physics, University of Oslo, Oslo, Norway, ⁶Birkeland Centre for Space Science, Bergen, Norway

Abstract Compared to the recently improved understanding of the nightside diffuse aurora, the mechanism(s) responsible for the dayside diffuse auroral precipitation remains limitedly understood. We investigate the dayside diffuse aurora observed by the all-sky imagers of Chinese Arctic Yellow River Station in the time interval of 02:00–10:00 UT (05:00–13:00 magnetic local time) on 2 January 2006. In this interval, the intensity of dayside diffuse aurora is highly correlated with the solar wind dynamic pressure with a maximum coefficient of 0.89. Moreover, there are similar spectra characteristics in the Pc5 range between the intensity of dayside diffuse aurora and solar wind dynamic pressure (proton density) during a portion of the time interval, in which the interplanetary magnetic field B_z is northward. The observation indicates that changes in solar wind dynamic pressure can efficiently modulate the magnitude of the dayside diffuse aurora, except when the interplanetary magnetic field is southward. The enhancement of the solar wind dynamic pressure can provide favorable circumstances for dayside chorus wave generation, so we consider that the dayside chorus could be a candidate for the production of the dayside diffuse aurora. Furthermore, since the compressional Pc4–Pc5 pulsations can also modulate the intensity of whistler mode chorus waves, the solar wind dynamic pressure modulates the dayside diffuse aurora through affecting dayside chorus wave activity and the associated scattering process.

1. Introduction

The diffuse aurora extends over a broad latitude range of 5° to 10° , mapping along the field lines from the outer radiation belts ($L \sim 4$) to the entire central plasma sheet with precipitation boundaries and peak location showing strong dependence on solar wind conditions. Different from the discrete aurora primarily caused by the parallel electron acceleration, the diffuse aurora dominantly originates from scattering by magnetospheric whistler mode chorus waves through resonant wave-particle interaction [Thorne *et al.*, 2010; Ni *et al.*, 2011a, 2011b, 2011c]. Using 11 years of particle data from the Defense Meteorological Satellite Program series satellites, Newell *et al.* [2009] reported that the diffuse aurora supplies the dominant energy deposit into the ionosphere during the conditions of both low and high solar wind driving. They showed that the diffuse aurora is more intense in postmidnight and into the morning hours and often relatively insignificant from postnoon through dusk, owing to the predominant eastward transport of electrons as a result of a combination of $E \times B$ and gradient drifting from the nightside plasma sheet. Since the diffuse aurora is an important source to the ionosphere, it is an essential linkage for the magnetosphere-ionosphere coupling.

Recent comprehensive theoretical and modeling studies in combination with the CRRES observations [Thorne *et al.*, 2010; Ni *et al.*, 2011a, 2011b] have demonstrated that scattering by electromagnetic whistler mode chorus waves is the dominant cause of the most intense diffuse auroral precipitation on the nightside-to-dawnside in the inner magnetosphere ($L < \sim 8$). Ni *et al.* [2012] also proposed that electrostatic electron cyclotron harmonic waves can be an important or even dominant driver of diffuse auroral precipitation in the nightside outer magnetosphere, through a detailed case investigation. Despite intensively improved understanding of the origin of nightside diffuse aurora, the mechanism(s) responsible for dayside diffuse aurora remains limitedly understood. In previous work [Shi *et al.*, 2012], we investigated a dayside diffuse auroral intensification event at the Chinese Arctic Yellow River Station (YRS). By computing the bounce-averaged resonant scattering rates with statistical information of dayside chorus, we suggested that whistler chorus could play a major role in the observed enhancement of dayside diffuse aurora. Nishimura *et al.* [2013] presented simultaneous observations of dayside diffuse aurora by South Pole all-sky imager and whistler mode waves by the Time History of Events

and Macroscale Interactions during Substorms spacecraft, which was followed by a comprehensive modeling analysis of *Ni et al.* [2014] that numerically confirmed that the observed dayside lower band chorus dominantly controlled the measured dayside diffuse auroral brightness and further supported the causal relationship between the whistler mode waves and the diffuse auroral pattern on the dayside.

In the present study, we analyze a representative event of dayside diffuse aurora observed by the all-sky imagers (ASI) at YRS, under the modulation impact of the solar wind dynamic pressure. Through a comprehensive correlation investigation, we demonstrate that the intensity of the dayside diffuse aurora was highly correlated with the solar wind dynamic pressure profile. Our reported modulation effect of the solar wind dynamic pressure on the dayside diffuse aurora strongly suggests that the latter largely rely on the dayside magnetospheric configuration and supports as well that dayside chorus, preferentially triggered by the marginal instability associated with ULF fluctuations [*Li et al.*, 2010, 2011], is important to the formation of the dayside diffuse aurora.

2. Observations and Analyses

The Chinese Arctic Yellow River Station (YRS) in Ny-Ålesund, Svalbard, is located at the geographic coordinates 78.92°N, 11.93°E with the corrected geomagnetic latitude 76.24° and magnetic local time (MLT) \approx UT + 3 h. Three identical all-sky imagers (ASI), supplied with the narrow band interferential filters centered, respectively, at N₂⁺ (1NG) 427.8 nm, O (1S) 557.7 nm, and O (1D) 630.0 nm, have been in operation since November 2003. The auroras at three wavelengths are shown in blue, green, and red colors, which mainly correspond to the precipitating electrons with energies above a few keV, 0.5 to a few keV, and less than 500 eV, respectively [*Hu et al.*, 2009, 2012]. The ASI temporal resolution is 10 s, including a 7 s exposure time and a 3 s readout time. In principle, the specific location and high-quality equipment of YRS provide a unique opportunity for instantaneous and long-term dayside auroral observations on the geomagnetically oriented dayside. The diameter of the all-sky field of view is about 1000 km. Spatial resolution is from \sim 1 km at the zenith to \sim 36 km at the horizon at an altitude of 150 km. Readers are referred to *Hu et al.* [2009] for the details of the YRS ASI and measurements.

For the dayside diffuse aurora event of interest, which occurred during the time interval of 02:00–10:00 UT on 2 January 2006, we show in Figure 1 the variations of interplanetary magnetic field (IMF) and solar wind parameters (B_x , B_y , B_z , solar wind speed, proton density, and dynamic pressure) from Advanced Composition Explorer (ACE, red line) and Operating Missions as Nodes on the Internet (OMNI, dark line) data and geomagnetic indices (*SYM-H* and *AE*), and the variations of the YRS ASI observed 557.7/630.0 nm auroral intensities along the magnetic meridian, respectively. The 427.8 nm auroral data are not available during this time period. The IMF and solar wind parameters from the OMNI database did not show much variation until 03:45 UT. At 03:45 UT, the IMF B_y and B_z components decreased, and the solar wind proton density and dynamic pressure enhanced dramatically by a factor of >2 within \sim 10 min, which was followed by the strong fluctuations. The geomagnetic indices (*SYM-H* and *AE*) also exhibited considerable changes. The dynamic pressure remained fluctuating until being placid again at 04:45 UT. Simultaneously, the IMF B_z component turned negative, which lasted for about half an hour. Around 06:30 UT, the dynamic pressure and proton density dropped suddenly and then became low after 07:50 UT. During this time period (03:20 UT \sim 07:50 UT), the solar wind velocity (Figure 1d) remained almost undisturbed (generally from 420 km/s to 440 km/s) compared to the proton density. Therefore, it is reasonable to conclude that the variation of the solar wind dynamic pressure was primarily attributed to changes in the solar wind proton density, which is subsequently used for analyses together with the ASI auroral intensity profile. Note that the *SYM-H* presented a temporal variation similar to the solar wind dynamic pressure during this period.

From 03:45 UT to 06:30 UT, two types of auroras are observed by the ASI: the discrete aurora is dominantly presented above -30° of the zenith angle (ZA), and the intense 557.7 nm diffuse aurora occurred below -30° ZA, with the timing consistent with the solar wind proton density enhancement. At around 04:55 UT, both discrete (above -30° ZA) and diffuse (below -30° ZA) auroral intensities enhanced dramatically. From 06:15 UT to 06:30 UT, three distinct peaks appeared between -80° ZA and -30° ZA.

To better manifest the distinct impact of the solar wind proton density on the dayside diffuse auroral intensity, we show the observed auroral intensity at different zenith angles (ZA = 0° , -60° , -65° , -70° , -75° ,

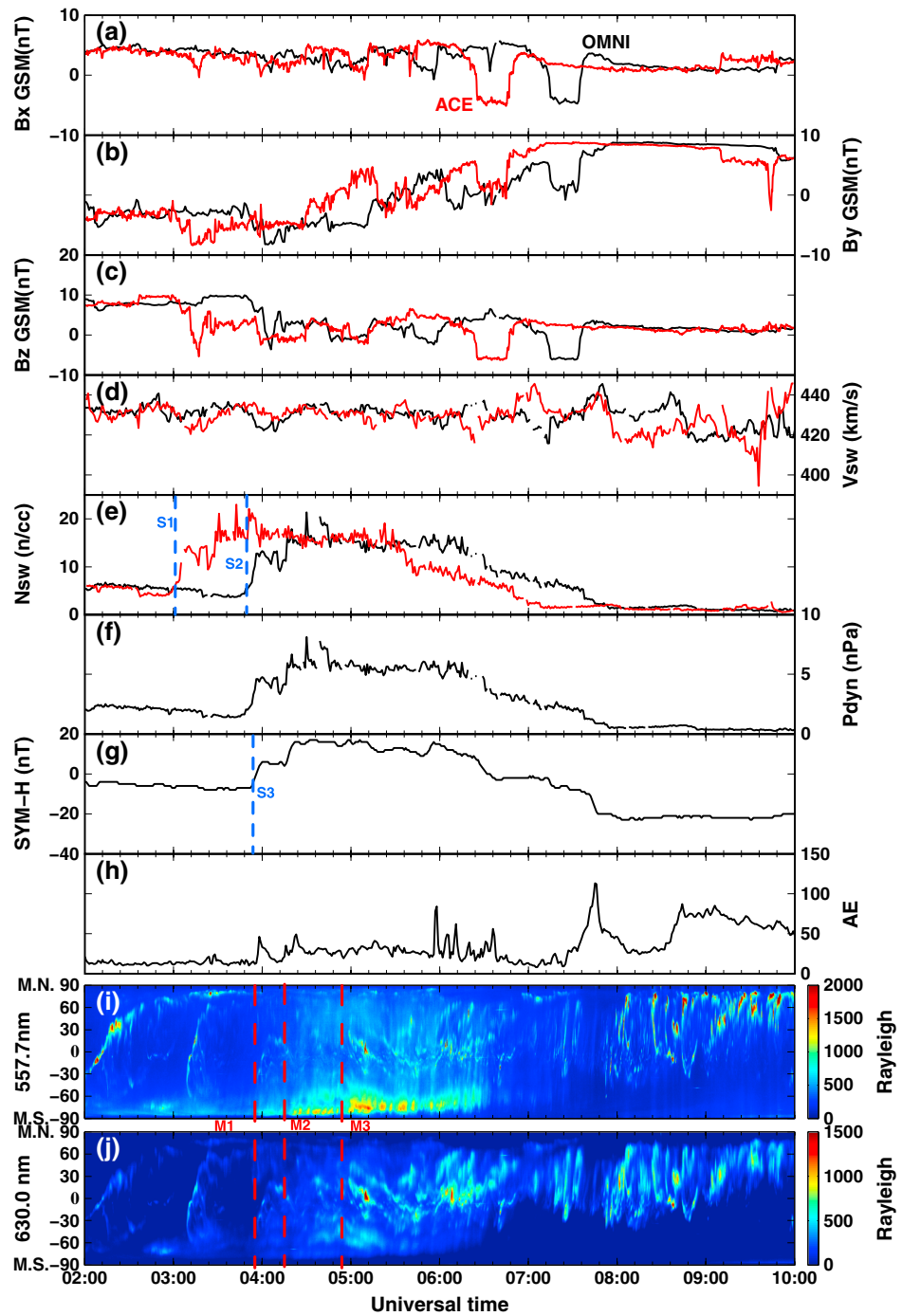


Figure 1. For the period of 02:00–10:00 UT on 2 January 2006, (a–h) IMF (B_x , B_y , and B_z), solar wind parameters (solar wind speed, proton density, and dynamic pressure) obtained from the ACE spacecraft (red line) and from the OMNIWeb (black line), geomagnetic indices ($SYM-H$ and AE), and (i–j) the keograms of the 557.7 nm and 630.0 nm emissions observed by the Chinese Arctic Yellow River Station (YRS) all-sky imagers. The vertical axis of Figures 1i and 1j gives the zenith angle (ZA) on the magnetic meridian (MS denotes magnetic south and MN denotes magnetic north). The horizontal axis shows the universal time (UT), which has about 3 h difference with the magnetic local time (MLT) at the YRS location.

and -80°) along with the solar wind parameters (the IMF B_z and the proton density) in Figure 2. To reach an optimal illustration, we have added different value to the auroral intensities at different ZA, as labeled in Figure 2b. It is discerned that the temporal variations of the auroral intensities and the solar wind proton density show high similarities, while a time difference tends to occur. As a consequence, we depict in

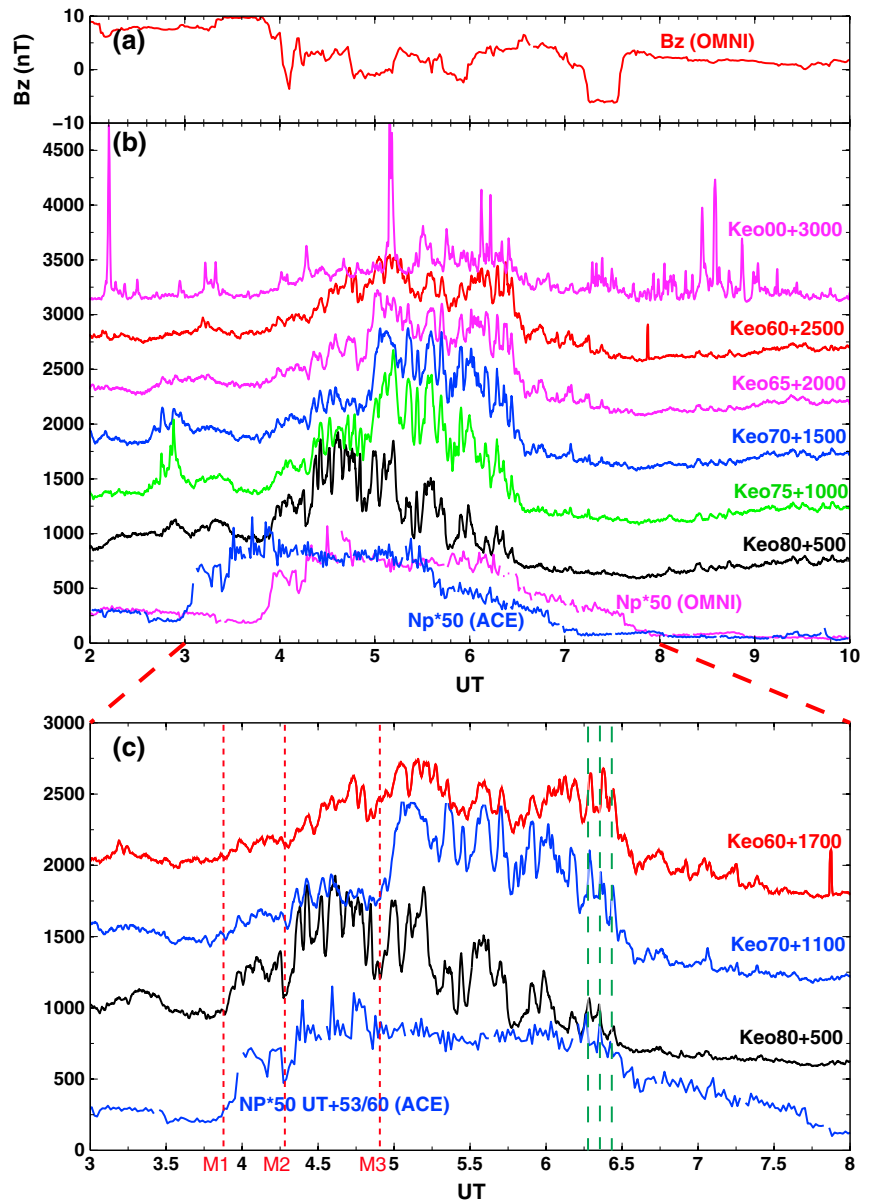


Figure 2. Temporal variations of (a) IMF B_z and of (b) the auroral intensities at different ZAs (i.e., 0° , -60° , -65° , -70° , -75° , and -80°) and the solar wind proton density obtained from ACE and OMNIWeb. Note that for illustration purpose, the actual values of the auroral intensities are artificially increased with a constant. For example, the label “Keo80 + 500” means that the value of the curve is the sum of the observed auroral intensity at $ZA = -80^\circ$ and a constant value of 500 Rayleigh. The solar wind proton density is multiplied by a factor of 50 and shown as blue for the ACE data and as pink for the OMNIWeb data. (c) Temporal variation of the auroral intensity at $ZA = -60^\circ$, -70° , and -80° and the ACE-measured solar wind proton density with a time lag of 53 min. The unit is rayleigh for the auroral intensity and cm^{-3} for the proton density. The vertical dashed green lines in Figure 2c give the three distinct enhancement of the proton density corresponding favorably to the peak of the auroral intensity peak, suggestive of a causal connection between them.

Figure 2c the auroral intensities at $ZA = -80^\circ$ (black), $ZA = -70^\circ$ (blue), and $ZA = -60^\circ$ (red) and the solar wind proton density (blue) from ACE during the period of 03:00–08:00 UT with a time lag of 53 min.

Because the ACE satellite is located at the L1 point, the solar wind detected by ACE undergoes certain travel time before it arrives at the Earth. In this case, the travel time from ACE to the nose of bow shock was about 48 min according to the first sudden enhancement of the solar wind proton density (e.g., dynamic pressure) shown in ACE (03:02 UT labeled as S1 in Figure 1e) and OMNI data (03:50 UT labeled as S2 in Figure 1e).

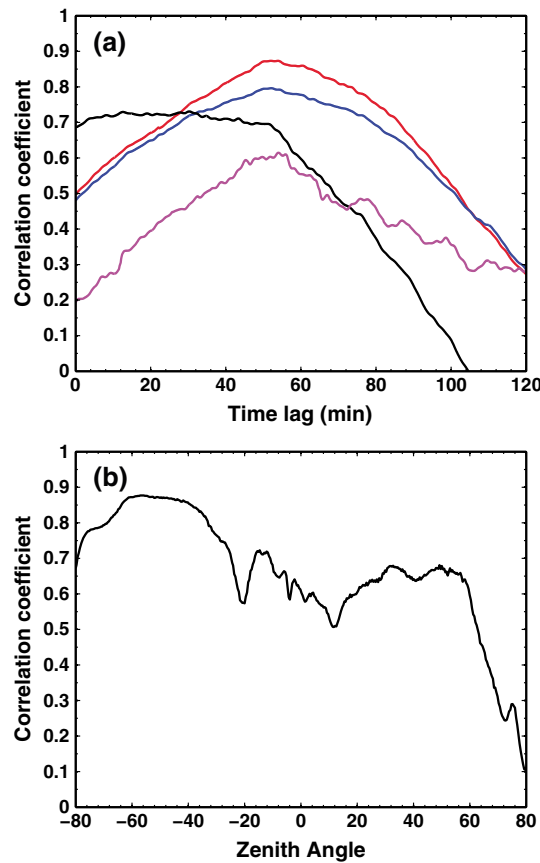


Figure 3. (a) Correlation coefficients between the solar wind proton density and the observed auroral intensity at -80° ZA (black), -70° ZA (blue), -60° ZA (red), and 0° ZA (pink) as a function of time lag (minute). (b) Correlation coefficients as a function of zenith angle with the time lag of 53 min.

coefficient is not maximal at -80° ZA (with a time lag of 53 min), the value still reaches 0.68. The correlation coefficient as a function of zenith angle with the time lag of 53 min is illustrated in Figure 3b. The coefficient value remains large below -30° ZA, with a maximum of 0.89, showing a high correlation between the solar wind dynamic pressure and the diffuse auroral intensity. Note that above -30° ZA, the discrete aurora tends to become important and even dominant, which can possibly explain the decrease of the correlation coefficient.

There is a sudden enhancement of the proton density around 03:55 UT (M1 in Figure 2c). Afterward, the proton density experienced a sudden decrease at 04:15 UT and a subsequent increase at 04:16 UT (M2 in Figure 2c). A similar trend of this temporal variation is also clearly shown in the observed auroral intensity at -80° ZA, and at -70° ZA and -60° ZA as well, although less distinctly. Note that the proton density has a valley between 03:30 UT and 03:55 UT, which is consistent with the decrease of the diffuse auroral intensity at -80° ZA and -70° ZA. Another example of modulation of the auroral intensity by the solar wind dynamic pressure occurred during the period between of 06:15 UT and 06:30 UT. In addition, all of the auroral intensities observed at different ZA showed periods of about 5 min (in the Pc5 range), which can also be seen from the proton density profile. As marked by the vertical dashed green lines in Figure 2c, each enhancement of the proton density corresponds favorably to the peak of the auroral intensity peak, suggestive of a causal connection between them.

Interestingly, the diffuse auroral intensity experiences a sudden enhancement around 04:55 UT at -60° ZA, -65° ZA, -70° ZA, -75° ZA, and even -80° ZA (M3 in Figure 2c), which, however, tends to be not attributed to the dynamic pressure increase since there was no obvious variation of the solar wind proton density. In addition, the discrete auroral intensity showed an intense enhancement between 0° ZA and 30° ZA in both 557.7 nm and 630.0 nm starting from 04:55 UT. Correspondingly, we see the inverse of the IMF B_z component at 04:46 UT (Figure 2a), which may trigger the magnetic reconnection on the dayside magnetopause, giving rise to

After 6 min, the *SYM-H* responded to the first sudden increase of the solar wind dynamic pressure (03:56 UT labeled as S3 in Figure 1g). However, for the dayside diffuse aurora, which was located below -30° ZA, the 557.7 nm auroral intensity was observed to increase suddenly at 03:55 UT (labeled as M1, red dashed line in Figure 1i). Moreover, a second sudden increase of the solar wind proton density (e.g., dynamic pressure) occurred at 03:23 UT in the ACE data, and there was also a second increase of the diffuse auroral intensity at 04:16 UT (labeled as M2, red dashed line in Figure 1i). Then, we consider that the response time of the dayside aurora for the sudden enhancement of the solar wind proton density (e.g., dynamic pressure) shown in ACE data is ~ 53 min. We think that the physics for such a time lag can result from a number of factors, e.g., the travel of solar wind toward the magnetosheath, the response of particle precipitation to geomagnetic disturbance, and the time scale for resonant wave-particle interactions. A quantitative evaluation of its physics requires future investigation, which, however, is beyond the scope of the present study.

Figure 3a gives the computed correlation coefficient as a function of assumed time lag (in minutes) at -80° ZA (black), -70° ZA (blue), -60° ZA (red), and 0° ZA (pink). The proton density data within the time window of 02:00–07:00 UT is used for correlation calculations. The correlation coefficients show peak values when the time lag is set as 53 min, reaching 0.88 at -60° ZA, 0.80 at -70° ZA, and 0.60 at 0° ZA. While the corresponding

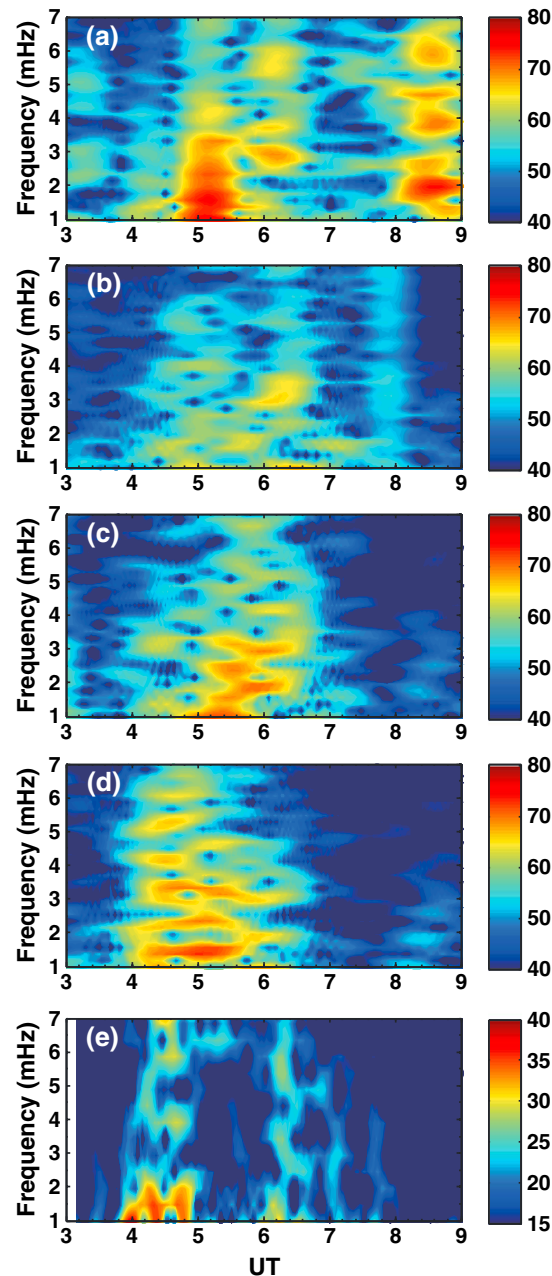


Figure 4. (a–d) The spectrograms of the auroral intensity as a function of UT and modulation frequency at 0° ZA, –60° ZA, –70° ZA, and –80° ZA. (e) The corresponding spectrogram of the solar wind proton density, after taking into account the time lag of 53 min.

06:15 UT. At 03:30 UT, there occurred a slight decrease of the solar wind proton density (with the time lag considered). Correspondingly, the diffuse auroral intensity also showed a decrease. Subsequently, the first sudden enhancement at 03:55 UT (M1 in Figure 2c) and the second at 04:16 UT (M2 in Figure 2c) and following temporal variation of the auroral intensity kept pace with the proton density variation until 04:55 UT (M3 in Figure 2c). During the interval of 03:30–04:55 UT, the IMF B_z is almost in the northward except a short period around 04:06 UT (Figure 2a). Starting from 04:55 UT, the proton density and the solar wind dynamic pressure remained at a high level ($\sim 15 \text{ cm}^{-3}$ and 5 nPa) and showed little variation. However, there occurred a sudden enhancement for the diffuse auroral intensity (M3 in Figure 2c), which just followed the

the particles injection from the magnetosheath to magnetosphere and consequently cause the variation of the dayside discrete and diffuse auroras.

To perform a comprehensive investigation of the intrinsic correlation between the observations of the auroral intensity and the solar wind dynamic pressure, we apply the Wavelet analysis. Figures 4a–4d depicts the spectrograms of the aurora intensity as functions of UT and frequency at 0° ZA, –60° ZA, –70° ZA, and –80° ZA, respectively. The spectrogram of the proton density with a time lag of 53 min is shown in Figure 4e. The comparison between Figure 4e and Figures 4a–4d indicates the effect of the solar wind on the auroral intensity. From 04:00 UT to 05:00 UT, the spectrum of the proton density (Figure 4e) has a peak value between 1 and 2 mHz, consistent with that of the diffuse auroral intensity at –80° ZA (Figure 4d). This corresponds to the high correlation between the variations of both quantities in that time period, i.e., simultaneous increases at 04:00 UT followed by the decrease and enhancement around 04:30 UT. Another representative spectrum is around 06:20 UT. The spectra of the proton density and the auroral intensity both show relatively large values at 3.5 mHz, which corresponds to the periodic variation at 06:20 UT (Figure 2b). Between 05:00 and 06:00 UT, the proton density spectrum shows a valley structure with much lower values for all frequencies, whereas the auroral intensity spectrum remains high especially at 0° ZA. We note that this time period corresponds to the presence of southward IMF B_z , suggesting that IMF B_z also play a significant role in affecting the intensity of the dayside diffuse aurora.

3. Discussion and Summary

We have shown a representative event of the dayside diffuse aurora, the intensity of which was highly modulated by the solar wind dynamic pressure. It was observed by the ASI at YRS on 2 January 2006. Three time intervals or stamps are emphasized: 03:30–04:55 UT, 04:55 UT, and

turning of IMF B_z from northward to southward at 04:46 UT. From 06:00 UT, when the IMF B_z was in the northward again, the diffuse auroral intensity changed with the variation of the solar wind proton density (i.e., the dynamic pressure), especially for the obvious three peaks around 06:15 UT. It is suspected that the dayside diffuse aurora is only controlled by the solar wind dynamic pressure when the IMF B_z is positive and can be affected by the negative IMF B_z when the solar wind dynamic pressure is at a high level.

The computed correlation coefficients between the diffuse auroral intensity and the solar wind dynamic pressure are high, indicating a causal relationship between these two phenomena. Recent studies [Shi *et al.*, 2012; Nishimura *et al.*, 2013; Ni *et al.*, 2014] have proposed that dayside chorus is a major contributor to the occurrence of the dayside diffuse aurora. Besides, the dynamic pressure enhancement can play as one favorable circumstance for dayside chorus generation/amplification [Li *et al.*, 2009, 2010]. Therefore, it is a natural and reasonable speculation, by combining these physical links, that the variation of the solar wind dynamic pressure, by driving dayside chorus for electron diffusion into the loss cone, plays a significant role in affecting the precipitation of the diffuse auroral electrons. Keika *et al.* [2012] showed that high solar wind pressure produces uniform B zone on the dayside, which provides a favorable condition for chorus wave excitation and thus enhanced the dayside diffuse aurora. Moreover, in the present event, the enhanced amplitudes of the dayside diffuse auroral intensity at different zenith angles are different with the enhancement of solar wind pressure at M1 and M2 (Figure 2c); i.e., the enhanced amplitude is large at -80° ZA and low at -70° and -60° ZA. It may be due to that the wave amplitudes of chorus wave are different at different L shells; namely, the wave amplitudes at low L shells are larger than those at higher L shells, which requires further investigations in following studies.

While Shi *et al.* [2012] reported another intense enhancement of the green line diffuse aurora acquired by the ASI of YRS in association with noticeable increases in the solar wind dynamic pressure, the present study shows clearly for the first time, as far as we know, the modulation of the diffuse auroral brightness by the solar wind dynamic pressure at frequencies in the Pc5 range. It is shown that the compressional Pc4-Pc5 pulsations produced by the solar wind dynamic pressure can cause the variation of the ratio of resonant electrons to the total electrons and in turn modulate the intensity of whistler mode chorus waves [Li *et al.*, 2011]. This effect tends to occur at large L shells of 8–12 in the dawn sector. Based on the close relationship between dayside diffuse aurora and whistler mode chorus waves result, the intensity of dayside diffuse aurora in the dawn sector driving by the chorus wave is also modulated by the compressional pulsations.

As mentioned above, the high solar wind pressure provides a favorable condition for chorus wave excitation, which can enhance the dayside diffuse aurora; however, there are also other factors which can affect the excitation of the dayside diffuse aurora, i.e., the total electron precipitation flux. In the present event, a turning of IMF B_z from northward to southward occurred at 04:46 UT. Then, more electrons should be injected into the magnetosphere from the magnetosheath by the magnetic reconnection in the dayside magnetopause. It causes the enhancement of the electron number in the closed-field magnetosphere and leads to the overall increase of the total electron precipitation flux and the diffuse auroral intensity. This might explain a sudden enhancement for the diffuse auroral intensity (M3 in Figure 2c), although the proton density and the solar wind dynamic pressure did not show a sudden increase. Nevertheless, the injecting electrons are dominantly in the outer closed-field magnetosphere, so the enhancement of the dayside diffuse auroral intensity at high latitudes ($-60^\circ \sim -70^\circ$ ZA) is more than at low latitude (-80° ZA), as shown in Figure 2c.

In the present study, we present in details that the solar wind proton density (i.e., the solar wind dynamic pressure) modulated favorably the intensity of the dayside diffuse aurora in the Pc5 range during one event, which we further explain as being causally connected to dayside magnetospheric fluctuations and dayside chorus wave scattering. However, there is no direct evidence, especially the simultaneous in situ wave measurements, to fully uncover how the modulation process operated. Pursuit of good conjugated ground-based and spaceborne measurements, including the solar wind, the auroral brightness, and the waves, will be the subject of our following investigation for comprehensive understanding of the underlying modulation mechanism.

References

- Hu, Z.-J., et al. (2009), Synoptical distribution of dayside aurora: Multiple-wavelength all-sky observation at Yellow River Station in Ny-Ålesund, Svalbard, *J. Atmos. Sol. Terr. Phys.*, *71*, 794–804, doi:10.1016/j.jastp.2009.02.010.
- Hu, Z.-J., H.-G. Yang, D.-S. Han, D.-H. Huang, B.-C. Zhang, H.-Q. Hu, and R.-Y. Liu (2012), Dayside auroral emissions controlled by IMF: A survey for dayside auroral excitation at 557.7 and 630.0 nm in Ny-Ålesund, Svalbard, *J. Geophys. Res.*, *117*, A02201, doi:10.1029/2011JA017188.

Acknowledgments

The OMNI data are from the OMNIWeb (<http://omniweb.gsfc.nasa.gov/>), and the ACE data are from the Coordinated Data Analysis Web (http://cdaweb.gsfc.nasa.gov/istp_public/). This research was supported by the National Natural Science Foundation of China (41274164, 41031064, 41004061, 41204120, 41474141, and 41374161) and Public Science and Technology Research Funds Projects of Ocean (201005017). Z.-J. H. acknowledges the financial support of the Chinese Arctic and Antarctic Administration (grant IC201205). B.N. also acknowledges the support from the Fundamental Research Funds for the Central Universities (grant 2042014kf0251). We also thank the reviewers for their careful examinations of and constructive comments on our manuscript.

Yuming Want thanks Mei-Ching Fok and another reviewer for their assistance in evaluating this paper.

- Keika, K., M. Spasojevic, W. Li, J. Bortnik, Y. Miyoshi, and V. Angelopoulos (2012), PENGUIn/AGO and THEMIS conjugate observations of whistler mode chorus waves in the dayside uniform zone under steady solar wind and quiet geomagnetic conditions, *J. Geophys. Res.*, *117*, A07212, doi:10.1029/2012JA017708.
- Li, W., R. M. Thorne, V. Angelopoulos, J. Bortnik, C. M. Cully, B. Ni, O. LeContel, A. Roux, U. Auster, and W. Magnes (2009), Global distribution of whistler-mode chorus waves observed on the THEMIS spacecraft, *Geophys. Res. Lett.*, *36*, L09104, doi:10.1029/2009GL037595.
- Li, W., et al. (2010), THEMIS analysis of observed equatorial electron distributions responsible for the chorus excitation, *J. Geophys. Res.*, *115*, A00F11, doi:10.1029/2009JA014845.
- Li, W., R. M. Thorne, J. Bortnik, Y. Nishimura, and V. Angelopoulos (2011), Modulation of whistler mode chorus waves: 1. Role of compressional Pc4-5 pulsations, *J. Geophys. Res.*, *116*, A06205, doi:10.1029/2010JA016312.
- Newell, P. T., T. Sotirelis, and S. Wing (2009), Diffuse, monoenergetic, and broadband aurora: The global precipitation budget, *J. Geophys. Res.*, *114*, A09207, doi:10.1029/2009JA014326.
- Ni, B., R. M. Thorne, R. B. Horne, N. P. Meredith, Y. Y. Shprits, L. Chen, and W. Li (2011a), Resonant scattering of plasma sheet electrons leading to diffuse auroral precipitation: 1. Evaluation for electrostatic electron cyclotron harmonic waves, *J. Geophys. Res.*, *116*, A04218, doi:10.1029/2010JA016232.
- Ni, B., R. M. Thorne, N. P. Meredith, R. B. Horne, and Y. Y. Shprits (2011b), Resonant scattering of plasma sheet electrons leading to diffuse auroral precipitation: 2. Evaluation for whistler mode chorus waves, *J. Geophys. Res.*, *116*, A04219, doi:10.1029/2010JA016233.
- Ni, B., R. M. Thorne, Y. Y. Shprits, K. G. Orlova, and N. P. Meredith (2011c), Chorus-driven resonant scattering of diffuse auroral electrons in nondipolar magnetic fields, *J. Geophys. Res.*, *116*, A06225, doi:10.1029/2011JA016453.
- Ni, B., J. Liang, R. M. Thorne, V. Angelopoulos, R. B. Horne, M. Kubyskhina, E. Spanswick, E. F. Donovan, and D. Lummerzheim (2012), Efficient diffuse auroral electron scattering by electrostatic electron cyclotron harmonic waves in the outer magnetosphere: A detailed case study, *J. Geophys. Res.*, *117*, A01218, doi:10.1029/2011JA017095.
- Ni, B., J. Bortnik, Y. Nishimura, R. M. Thorne, W. Li, V. Angelopoulos, Y. Ebihara, and A. T. Weatherwax (2014), Chorus wave scattering responsible for the Earth's dayside diffuse auroral precipitation: A detailed case study, *J. Geophys. Res. Space Physics*, *119*, 897–908, doi:10.1002/2013JA019507.
- Nishimura, Y., et al. (2013), Structures of dayside whistler-mode waves deduced from conjugate diffuse aurora, *J. Geophys. Res. Space Physics*, *118*, 664–673, doi:10.1029/2012JA018242.
- Shi, R., D. Han, B. Ni, Z.-J. Hu, C. Zhou, and X. Gu (2012), Intensification of dayside diffuse auroral precipitation: Contribution of dayside whistler-mode chorus waves in realistic magnetic fields, *Ann. Geophys.*, *30*, 1297–1307.
- Thorne, R. M., B. Ni, X. Tao, R. B. Horne, and N. P. Meredith (2010), Scattering by chorus waves as the dominant cause of diffuse auroral precipitation, *Nature*, *467*, 943–946, doi:10.1038/nature09467.